Research Paper

Evolution of mammalian longevity: age-related increase in autophagy in bats compared to other mammals

Joanna Kacprzyk[1,*], Andrea G. Locatelli[1,3,*], Graham M. Hughes[1,*], Zixia Huang[1], Michael Clarke[1], Vera Gorbunova[2], Carlotta Sacchi[1], Gavin S. Stewart[1], Emma C. Teeling[1]

[1]School of Biology and Environmental Science, University College Dublin, Belfield, Dublin 4, Ireland
[2]Departments of Biology and Medicine, University of Rochester, Rochester, NY 14627, USA
[3]Present Institutional Address: Division of Genetics and Cell Biology, Fondazione Centro San Raffaele, Via Olgettina, Milano 6020132, Italy
*Equal contribution

Correspondence to: Emma C. Teeling; **email:** emma.teeling@ucd.ie
Keywords: autophagy, bats, aging, blood mRNA, phylogenomics
Received: October 16, 2020 **Accepted:** March 5, 2021 **Published:** March 21, 2021

ABSTRACT

Autophagy maintains cellular homeostasis and its dysfunction has been implicated in aging. Bats are the longest-lived mammals for their size, but the molecular mechanisms underlying their extended healthspan are not well understood. Here, drawing on >8 years of mark-recapture field studies, we report the first longitudinal analysis of autophagy regulation in bats. Mining of published population level aging blood transcriptomes (*M. myotis*, mouse and human) highlighted a unique increase of autophagy related transcripts with age in bats, but not in other mammals. This bat-specific increase in autophagy transcripts was recapitulated by the western blot determination of the autophagy marker, LC3II/I ratio, in skin primary fibroblasts (*Myotis myotis, Pipistrellus kuhlii*, mouse), that also showed an increase with age in both bat species. Further phylogenomic selection pressure analyses across eutherian mammals (n=70 taxa; 274 genes) uncovered 10 autophagy-associated genes under selective pressure in bat lineages. These molecular adaptations potentially mediate the exceptional age-related increase of autophagy signalling in bats, which may contribute to their longer healthspans.

INTRODUCTION

Understanding the aging process with a view of managing/reducing its ailments is crucial to improve the quality of life of our aging populations [1]. The hallmarks of aging are remarkably similar across mammals, but the rate vastly differs [2] and the molecular basis for this natural variation in longevity is not well understood. This suggests that studying the aging process in exceptionally long-lived species, such as bats, will enable us to elucidate the mechanisms underlying naturally evolved longer healthspans and ultimately contribute to a greater understanding of aging biology [3]. Relative to body mass, bats show the longest lifespans of all mammals and exhibit little signs of senescence [4, 5]. For this reason, bats are now being recognised as novel, relevant models to study the mechanisms of healthy aging. Comparative studies focused on bats have furthered our understanding of variation in aging across the mammal tree of life and suggested factors that may underlie their extended healthspans: telomeres [5], mitochondria [6], microbiome [7] and metabolome [8]. A recently published longitudinal study highlighted that bats exhibit a unique, age-related gene expression pattern associated with DNA repair, immunity and autophagy [9]. Indeed, autophagy and proteostasis were previously suggested to be the common mechanisms that maintain

health in long-lived species, including bats [10–12]. Enhanced autophagy has also been suggested as an anti-viral mechanism in *Rousettus* bats [13] which may also contribute to bat's unique longer healthspans [14]. However until now, studying the age-dependent changes of autophagy in wild bat populations has been hindered by the logistical challenges [5].

Autophagy is a convergent mechanism of multiple longevity pathways, playing a role in lifespan extension promoted by reduced insulin/IGF-1, mTOR inhibition and dietary restriction in mammals [15]. Functional studies in model species demonstrate that reduced autophagy shortens lifespan, while increased autophagy extends it [16]. Accordingly, many studies have demonstrated that autophagy decreases with age, and it has been inferred that this gradual decrease could play a major role in the functional deterioration of aging organisms [17].

To ascertain if autophagy is involved in bats' exceptional longevity, we firstly mined our published longitudinal bat blood transcriptomes [9] and identified 26 autophagy-associated genes that are up-regulated with age in long-lived wild *M. myotis* (Greater mouse-eared bat), but down-regulated in human and mouse. Secondly, drawing on two long-term mark-recapture studies of wild populations of *Myotis myotis* and *Pipistrellus kuhlii* (Kuhl's pipistrelle), we sampled wing-biopsies from bats across known ages, generated primary fibroblast cell lines, and demonstrated the increase of the autophagy marker, LC3II/I ratio, with age in both bat species, but not in mice. In order to identify the genomic adaptations underlying this unique age-related increase of autophagy signalling in bats, we carried out a eutherian-wide (n=70 species, including both *M. myotis* and *P. kuhlii* bats) comparative phylogenomic analyses of 274 autophagy-associated genes. Despite the high conservation of autophagy pathways, 10 genes showed unique evolutionary signatures of selection in bat lineages. These integrative data provide a multi-layered insight into bats' autophagy signalling and suggest that molecular adaptation of autophagy pathways may underly bats longer healthspans.

RESULTS

Bat-specific changes in expression of autophagy-associated genes with age

To explore the age-related changes in expression of autophagy associated genes we mined the aging blood transcriptomes from *M. myotis*, human and mouse that were previously generated in our lab [9]. The Spearman's rank correlation coefficients were extracted for 70 autophagy associated genes present in the dataset and pathway analysis suggested that autophagy GO terms show different patterns during aging in bats, compared to humans and mice (Table 1A). In particular, 26 genes showed increasing expression with age in *M. myotis* bats, while they were downregulated in both humans and mice (Table 1B).

LC3II/I ratio increases with age in bat skin-derived fibroblasts

The age-associated changes in LC3II/I ratio under control and serum withdrawal conditions were investigated using western blot in primary fibroblasts derived from female individuals. The experiments were limited to females since the bat captures were carried out in the maternity roosts and as a result the sampled individuals were predominantly female. The two bat species included in this study live longer than expected given their body mass. The calculated longevity quotient (LQ=observed/expected longevity) was 1.6 for *P. kuhlii* and 5.7 for *M. myotis*, in contrast to 0.6 for mouse, included as a control system. Wing skin biopsies (bats) or small ear skin (mouse) clippings were successfully used as a source of primary fibroblasts, with between 200 to 600k cells obtained per sample after 9-10 days of culture. In the pilot experiments, attempts to expand the fibroblast cultures beyond this point often resulted in reduced growth rate, therefore cells were not passaged further. Generally, samples from 6+ and 7+ years old *P. kuhlii* and 22-month old mouse grew at similar rate to the rest of the age ranges, but a smaller number of initial fibroblasts growth halos were produced, resulting in the lower final cell numbers available for experiments.

LC3II/I ratio measures conversion of the microtubule-associated protein 1 light chain 3 (LC3), from a free LC3I form to lipidated LC3II form associated with autophagosomes. As anticipated, skin-derived fibroblasts of all species (*P. kuhlii*, *M. myotis* and *M. musculus*) responded to serum withdrawal treatment with increase of LC3II/I ratio (Figure 1A). The increase of LC3II/I ratio in *M. myotis* and *P. kuhlii* fibroblasts induced by pharmacological treatment with rapamycin, another classic inducer of autophagy [18] additionally validated the use of this autophagy marker in bats (Supplementary Figure 1).

We avoided direct cross-species comparisons and focused on age-related changes within each species, as there might be species-specific differences in antibody affinity for LC3-I compared to LC3-II. The starvation-induced LC3II/I fold-change was not correlated with age in either bat species nor in mouse (Figure 1B). However, the basal LC3II/I ratio significantly increased

Table 1A. Comparative transcriptomic analyses between bat, human, mouse.

			Bat	Human	Mouse
GO:0006914	autophagy	62	0.194	-0.095	-0.003
GO:0016236	macroautophagy	47	0.197	-0.116	-0.026
GO:0010508	positive regulation of autophagy	16	0.204	-0.05	-0.05
GO:0010506	regulation of autophagy	44	0.196	-0.065	-0.018
GO:0016241	regulation of macroautophagy	25	0.209	-0.083	-0.05

Table 1B. Comparative transcriptomic analyses between bat, human, mouse.

Gene	Bat	Human	Mouse
PIK3CA	0.483	-0.233	-0.568
ROCK1	0.468	-0.091	-0.41
RB1CC1	0.446	-0.143	-0.164
CSNK2A1	0.415	-0.015	-0.406
NEDD4	0.383	-0.043	-0.1
PAFAH1B2	0.293	-0.278	-0.097
USP33	0.278	-0.237	-0.165
TRAPPC8	0.274	-0.167	-0.066
ULK2	0.271	-0.017	-0.312
SIRT1	0.243	-0.091	-0.566
SNX14	0.214	-0.27	-0.158
VTA1	0.208	-0.302	-0.327
MAP3K7	0.203	-0.213	-0.247
TBK1	0.198	-0.218	-0.215
VPS36	0.179	-0.207	-0.483
NRBF2	0.177	-0.236	-0.361
DNM1L	0.168	-0.081	-0.245
UBXN2B	0.146	-0.14	-0.179
EIF2AK4	0.141	-0.069	-0.361
SH3GLB1	0.132	-0.149	-0.039
PIK3R4	0.11	-0.227	-0.457
ATP6V1H	0.099	-0.172	-0.032
PIK3C3	0.077	-0.268	-0.269
RAB3GAP1	0.053	-0.013	-0.567
ATP6V1C1	0.03	-0.186	-0.09
U2AF1	0.03	-0.053	-0.207

(A) Comparison of the pathway expression pattern for autophagy-associated GO terms. Within each species, the median of the Spearman's correlation coefficients of all genes under each of enriched age-associated GO terms was used to represent their overall expression pattern with age. The values behind the GO terms indicate the number of genes enriched. (B) The autophagy associated genes that exhibited the opposite direction of expression changes with age in bat compared to human and mouse are shown. Values indicate the Spearman's correlation coefficients between gene expression and age for each species.

with age in *P. kuhlii* and *M. myotis*, but not in mouse (Figure 1C). Lack of LC3II/I increase with age in mice did not change after including samples from different genetic backgrounds, nor when derived from flank skin rather than ear skin [19] (Supplementary Figure 2). Total LC3 signal (LC3II + LC3I normalized to GAPDH) did not show age-related changes in any of the tested species (Figure 1D).

Increased LC3II/I ratio can be a result of either upregulation of autophagosome formation or a blockage of autophagic degradation [20]. To determine if the age-related increase of LC3II/I ratio observed results from defective autophagic degradation, we used bafilomycin A1 (Baf A1), an inhibitor of fusion between autophagosomes and lysosomes [21]. Both the basal and starvation-induced LC3II/I ratio significantly increased

in the presence of Baf A1 in *M. myotis* (Figure 2A). Moreover, there was no significant age-associated change in the effect of Baf A1 on the basal LC3II/I ratio (Figure 2B), indicating that the age-related increase in basal LC3II/I ratio was likely not due to defective autophagy. Due to low numbers of cells obtained for the oldest cohort of *P. kuhlii* (6-8 years) it was not possible to include the autophagy inhibitor treatment for this species. Representative gels for all experiments are included in the Supplementary Figure 3.

Assembly of *P. kuhlii* transcriptome

Given the lack of an assembled *P. kuhlii* genome, we isolated coding sequences (CDSs) of autophagy-associated genes suitable for selection tests, from our sequenced *P. kuhlii* fibroblast transcriptomes. To maximize the chance of capturing transcripts up- and down- regulated upon induction of autophagy, both control (n=3) and serum-starved (n=3) samples were sequenced (Supplementary Table 1A). *De novo*

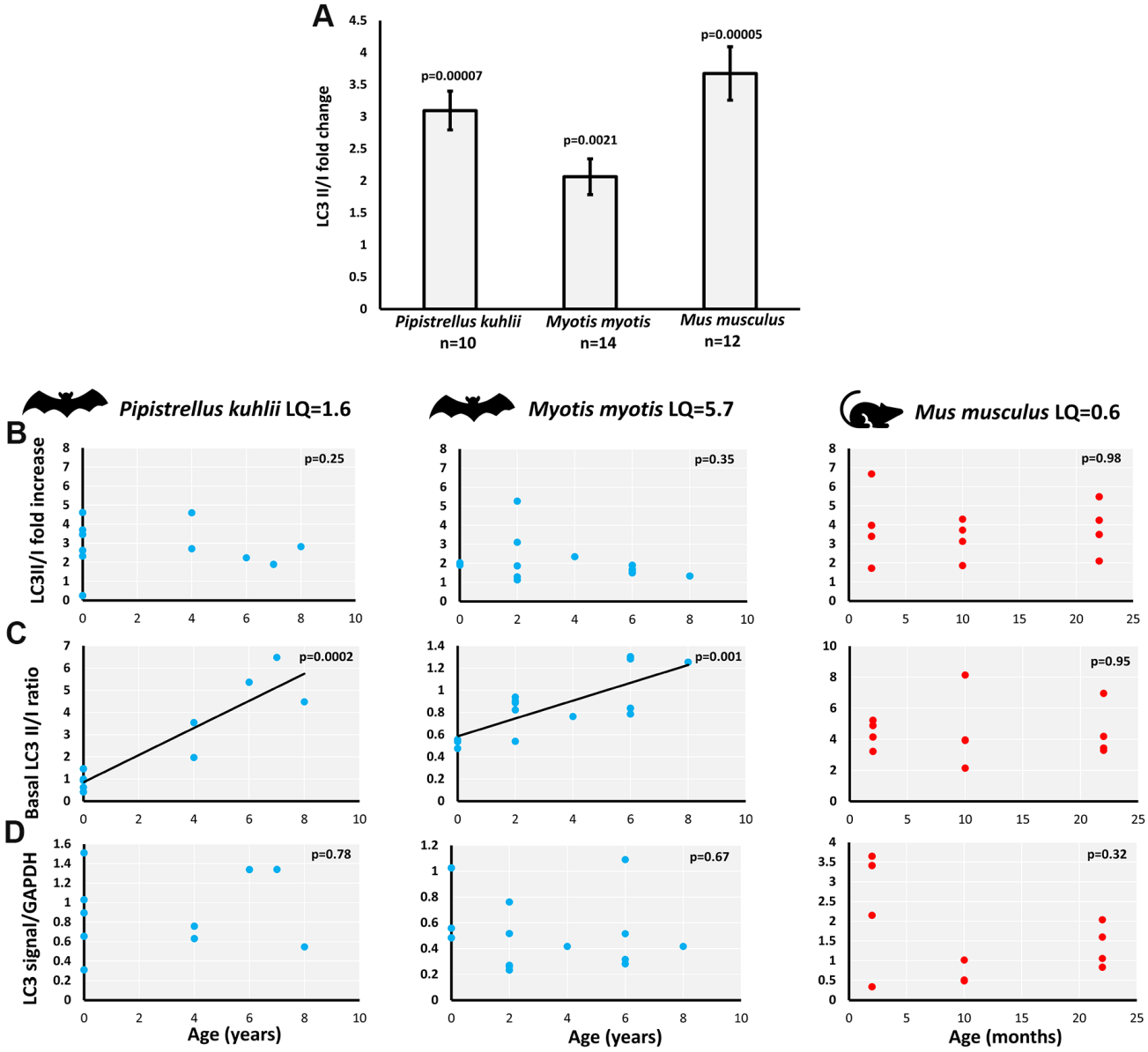

Figure 1. Basal and starvation-induced autophagy in skin-derived fibroblasts from *P. kuhlii*, *M. myotis* and *M. musculus*. (**A**) fold change of LC3 II/I ratio induced by serum withdrawal (p-values: two-tailed t-test; data represent mean ±SEM). Relationship between individual's age and (**B**) starvation-induced LC3II/I fold change, (**C**) basal LC3 II/I ratio, (**D**) GAPDH normalized total LC3 signal. (**B**–**D**) Corresponding *p*-values indicate the significance of linear model and are indicated in the top right-hand corner of each plot. Models are plotted where significant. LQ – longevity quotient. Note that scales differ between species.

pooled transcriptome assembly yielded a total of 271,767 transcripts (Supplementary Table 1B), of which 109,942 were annotated as protein-coding, corresponding to 15,542 unique genes. Twenty-four percent of autophagy associated genes retrieved using search term 'autophagy' from AmiGO database [22], exhibited differential expression under serum starvation conditions (Supplementary Table 2).

The signatures of positive and divergent selection in autophagy-associated genes in bats

Phylogenomic selection tests were carried out on a suite of autophagy associated genes across eutherian mammals. Tested genes were: i) GO-associated with term autophagy; ii) represented by at least 50% of the 62 mined eutherian genomes; and, iii) detected in the assembled *P. kuhlii* transcriptome. Supplementary Figure 4 presents the outline of workflow used to isolate the final set of 274 genes for selection analyses. Tests of positive and divergent selection were carried out independently along the bat lineages and mouse (Supplementary Figure 5). CodeML calculates the likelihood-derived dN/dS rates (ω), where dN is defined as a number of non-synonymous substitutions per non-synonymous sites and dS is a number of synonymous substitutions per synonymous sites. Positive selection (ω >1) was detected in *ATG9B* along the ancestral bat branch and for *LARP1* along the ancestral vespertilionid branch, with both genes showing significant sites under selection (Figure 3A, 3B and Supplementary Table 4). A number of sites had significant BEB scores for *ATG9B* in the *Myotis* ancestral branch, however these were present only in *M. lucifugus*, and represented a missing exon in other *Myotis* taxa. Within the individual lineages, positive selection was found in VMP1 and ZDHHC8 for *P. kuhlii*. Divergent selection was detected in MFN2 (ancestral bat branch) and in *MTOR, STOM, VPS4A* and *NPC1* (ancestral vespertilionid branch) (Figure 3C, 3D and Supplementary Table 3). The ω values for *MFN2, MTOR, STOM, VPS4A* were >1 in the foreground and <1 in the background

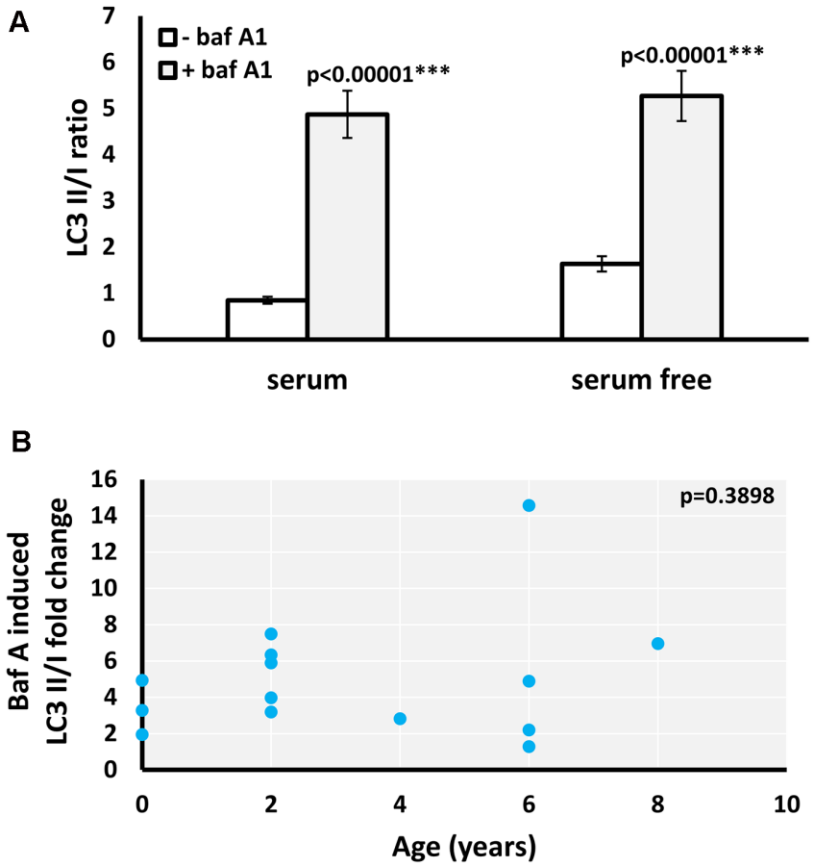

Figure 2. Effect of baf A1 autophagy block on basal and serum withdrawal-induced autophagic flux in *M. myotis* fibroblasts. (**A**) Basal and starvation-induced LC3II/I ratio in absence and presence of 100nM baf A1, data represent means ±SEM for n=14 individuals age 0 to 8. p-values (two-tailed t-test) indicate statistically significant effect of baf A1 treatment. (**B**) Relationship between individual's age and baf A1 induced fold change of basal (serum present) LC3II/I ratio (p-value included in the top right-hand corner of the plot indicates that linear model is not significant).

branch, indicating positive divergent selection acting along respective foreground branches. However, for *NPC1* both foreground and background ω fell within the region of purifying selection with values of 0.12 and 0.24 respectively, suggesting that this gene may be under extreme evolutionary constraint and thus essential for normal cellular function. In the individual lineages, divergent selection was found in *SFRP4* for the *P. kuhlii* (foreground ω>1, background ω<1). No genes found under selection in bats were found under selection in *M. musculus*, where positive selection was found in *PSAP* and divergent selection was found in *SNX14* (foreground ω<1, background ω>1) (Supplementary Table 3) showing different evolutionary pressures acting on autophagy pathways in bats and mice.

The network analysis (STRING database v.10. [23]) showed direct interaction between 5 genes under selection in the bat lineages (*LARP1*, *MTOR*, *ATG9B*, *VPS4A* and *MFN2*), and with 17 of autophagy-associated genes which positively correlated with age, and with the LC3 protein (Figure 4). This network showed a significant functional enrichment (FDR corrected p-value <0.05) for 152 Biological Process GO terms and 14 KEGG (Kyoto Encyclopedia of Genes and Genomes) pathways (Supplementary Tables 4, 5), including terms/pathways involved in the regulation and early events of autophagic activity.

DISCUSSION

The essential role of autophagy in lifespan regulation is supported by extensive evidence from studies on model species, including mouse, nematodes and flies, as well as humans [16, 24]. Autophagy is now one of the most studied phenomena in cell biology and pathophysiology, being explored as a therapeutic target of clinical interventions against aging and age-related diseases [24]. Studies investigating autophagy in non-model, remarkably long-lived species, like bats, may inform research to modulate autophagy for life extension purposes in humans. In the recent longitudinal study, autophagy was among the GO terms showing

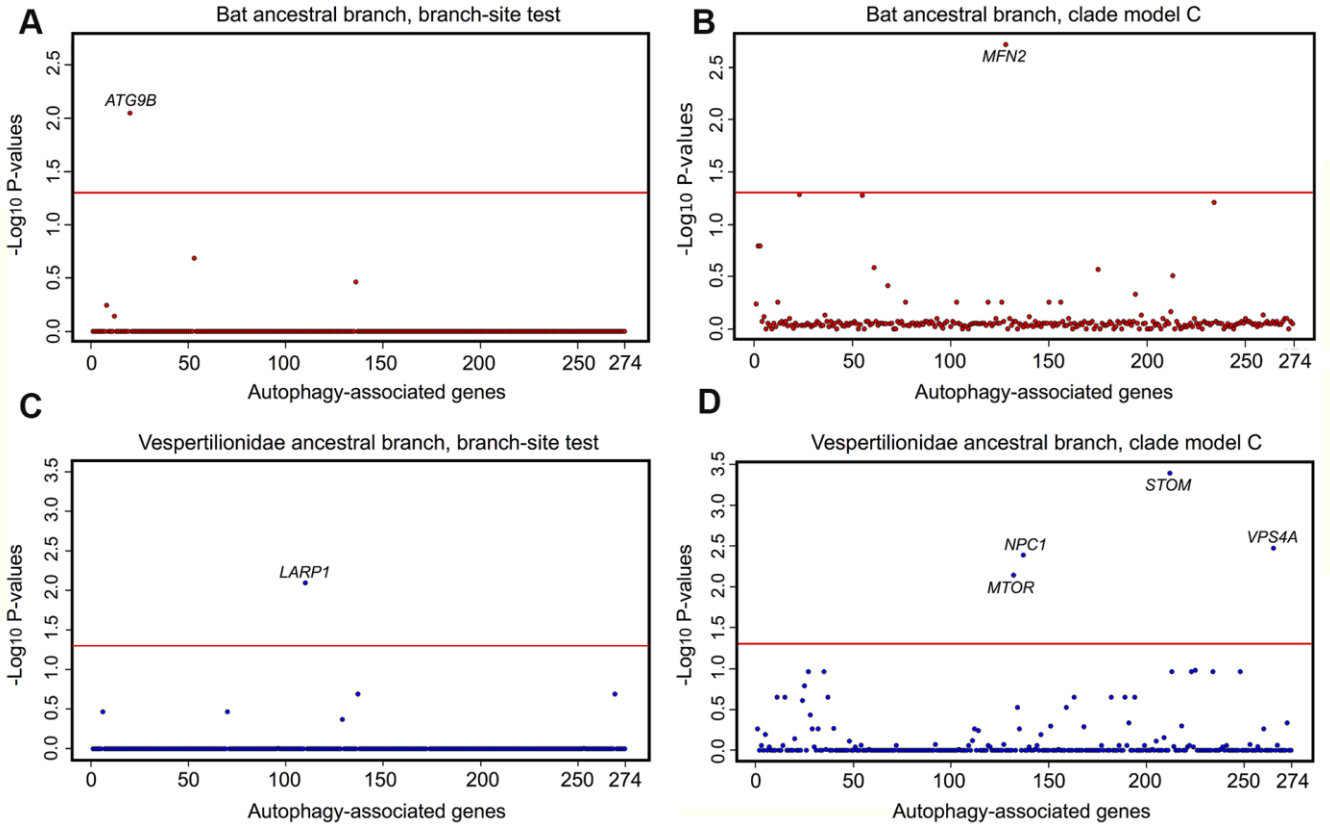

Figure 3. Selective pressure acting on autophagy-associated genes (n=274) in bat lineages. Results of tests for positive and divergent selection using the CodeML branch-site and clade model C models, conducted on the (**A**, **C**) the bat ancestor branch, (**B**, **D**) the vespertilionid ancestor. *P* values are transformed using $-\log_{10}$. Genes significant after FDR correction and appearing in both RefSeq and RefSeq+MAKER (including extra 8 species with highly fragmented genome assemblies) data sets are labelled above the red line, which indicates a significance cut-off of α = 0.05.

positive correlation with age in *M. myotis* blood transcriptomes [9]. Here, we highlight that the strong increase of autophagy-associated GO terms with age in bats, contrasts with decrease observed in human and mouse blood transcriptomes. Many of the identified 26 autophagy genes that positively correlated with age in bats, in contrast to downregulation observed for other mammals, were previously experimentally proven to promote autophagy and directly linked to longevity and age-related diseases by functional studies, e.g. *RB1CC1* [25], *NEDD4* [26], *ULK2* [27], *SIRT1* [28], *DNMIL* [29] and *ATP6V1H* [30].

The age-related increase of autophagy in wild bat blood transcriptomes was mirrored by the increase in marker of autophagy, LC3II/I ratio, observed in skin-derived fibroblasts of *P. kuhlii* and *M. myotis*, which live longer than expected considering their body size. In contrast, skin-derived fibroblasts from the short-lived mouse did not show a similar increase. The data support the hypothesis that bats maintain their ability to ensure cellular homeostasis through efficient removal of cellular damage as they age. It is generally accepted that aging results from the accumulation of cellular damage promoted by chronic stress, and autophagy, being the stress sensor mechanism, attenuates age-associated processes and mediates cytoprotection [31]. In old age, activity of the autophagy machinery is insufficient, either because the autophagic flux is diminished or because there is too much cargo resulting from chronic cellular damage [24]. The increase in expression of autophagy-associated genes and the increased LC3II/I ratio observed in older bats may indicate that their autophagic machinery efficiently removes the higher levels of age-associated cellular damage, which in turn contributes to their longevity. The increased expression of autophagy-associated transcripts with age may be also a compensation response for impaired autophagic

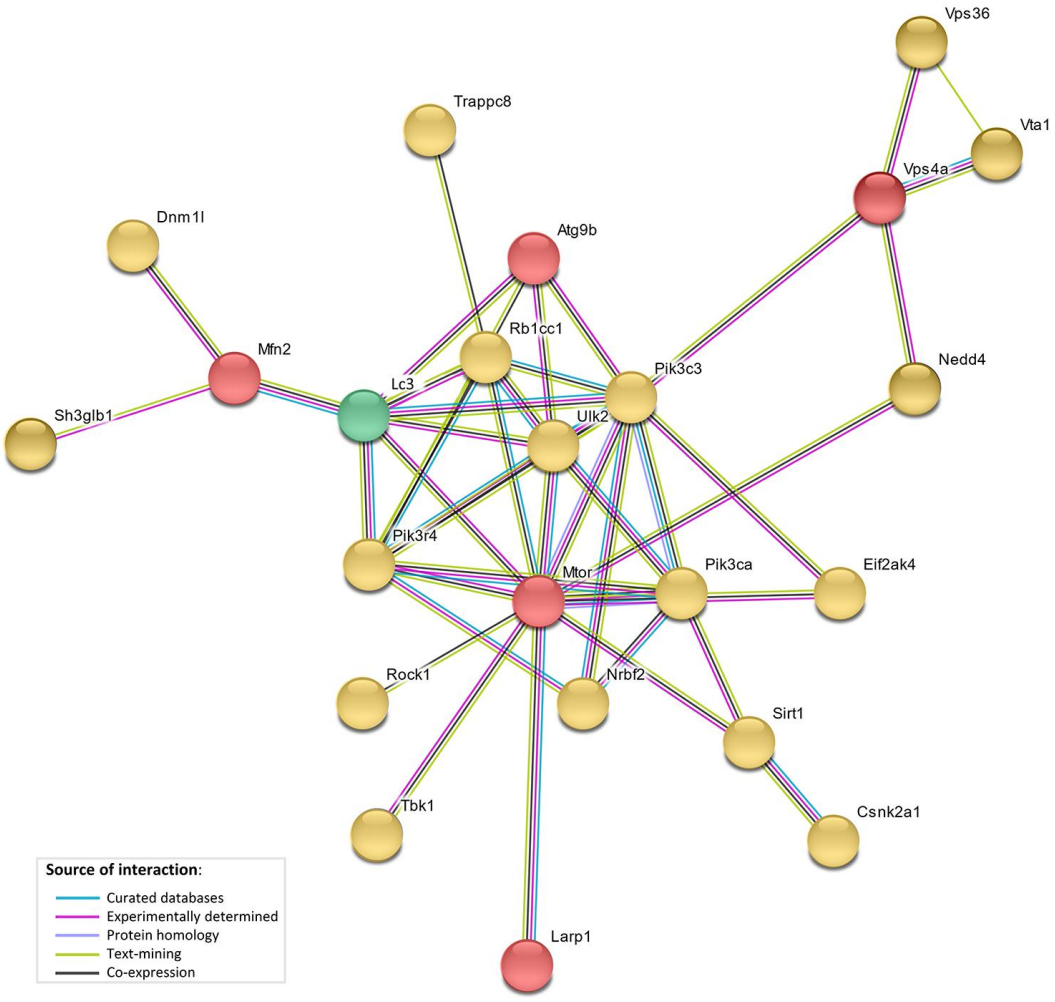

Figure 4. STRING interaction network. STRING protein-protein interaction network showing direct interactions between genes under selective pressure in bat lineages (red), genes with bat-specific upregulation with age (yellow), and LC3 (green).

degradation (potentially indicated by higher LC3II/I ratio in older animals). However, our experiments with the autophagy inhibitor, bafilomycin A1, do not support this interpretation, at least for *M. myotis*. In contrast to bat species, downregulation of autophagy-associated genes in human and mouse and the lack of increase in LC3II/I ratio in fibroblasts derived from aged mice (22 months, representing approx. 85% of average life span in captivity; [32]) suggests that in mice, the basal autophagic activity is not adjusted to deal with the higher level of age-associated cellular damage. Similarly, the lack of increased autophagy in aged dermal fibroblasts has been recently proposed to contribute to skin aging in humans [33]. Indeed, reduced expression of autophagy-related genes occurs with age and leads to increases in oxidative stress and aberrant protein accumulation in a *Drosophila* model of Alzheimer's disease [34]. Increased sensitivity of bat autophagy pathways to cellular damage is also plausible in the light of the proposed link between flight and longevity [35, 36]. Flight is associated with a high metabolic rate and an increased risk of oxidative damage, therefore its acquisition may have driven an evolutionary 'counter-balance' adaptation of cytoprotective pathways, like autophagy, promoting healthspan extension in bats. Future studies on multiple longer and shorter-lived bat species with varying life history strategies will further explore the role of autophagy in driving bats longevity.

We used a comparative phylogenomics approach to identify the evolutionary adaptations underlying the age-related increase of autophagy activity in bats. Evidence of positive and divergent selection was rare along all tested branches, as expected due to evolutionary constraint on protein-coding genes and in line with the recent large-scale study investigating evolutionary selection in bat lineages that revealed positive selection in <1% of genes investigated [37]. The paucity of positive and divergent selection observed was also expected given conservation of the autophagy pathways across vertebrates [38]. There were, however, several exceptions. Significant amino acid sites showing positive selection were detected along the ancestral bat and ancestral vespertilionid branches for *ATG9B* and *LARP1*, respectively. The ATG9 complex is a multimembrane-spanning autophagy regulator and its expression was also previously reported to reduce the conversion of LC3 [39]. LARP1 stabilizes transcript of *MTOR* [40], which is a potent autophagy inhibitor and a key protein implicated in lifespan regulation [41]. *MTOR* itself, as well as *STOM*, encoding the lysosomal integral membrane protein stomatin [42] and *VPS4A*, involved in lysosomal/endosomal membrane trafficking and autophagosome completion [43] were found to be under divergent selection along the ancestral vespertilionid branch. Intriguingly, *VPS4A* has recently shown a significant correlation with the longevity in the comparative transcriptome study across 16 mammals [44]. *MFN2*, that modulates the ER/mitochondria connections regulating mitochondrial supply of membranes for autophagosome biogenesis [45], showed evidence of sequence divergence in bats relative to other mammals. *MFN2* levels decrease with age and *MFN2* ablation in mice generates a gene signature linked to aging by reducing autophagy [46]. We found evidence of positive selection in *VMP1*, required for autophagosome function [47] and *ZDHHC8*, involved in metabolism pathways [48] in *P. kuhlii*. No evidence of positive selection was found for these genes in the mouse lineage, suggesting a bat-specific pattern of sequence evolution in autophagy-related genes, which may underlie their extended longevity.

Molecular adaptations of the genes identified by our phylogenomic selection pressure tests in the ancestral bat and vespertilionid lineages may drive the age-related increase of autophagic activity in *M. myotis* and *P. kuhlii*. In this study, the *LARP1* and *STOM* are for the first time implicated in an aging context. Our STRING-Protein association network analyses predicted direct interactions between a number of gene products highlighted by our phylogenomic, transcriptomic and cell culture analyses. This suggests functional divergence of the proteins under selection in the bat lineages, implying that they may drive the age-related increase in autophagy signalling observed at the transcriptome and protein level. Further studies are required for functional validation of these findings. For example, knock-ins of bat *ATG9B* or *MFN2* (under selection in ancestral bat lineage) in mouse, or another model species, could be generated to examine the effect of bat-specific adaptations in these genes on the transcriptomic profiles and autophagy activity associated with conditions inducing cellular damage or indeed senescence.

In conclusion, we present an approach based on non-lethal and minimally invasive sampling, offering an unprecedented opportunity to probe the age-dependent autophagy markers in wild transponded bat populations. By integrating comparative cell biology, transcriptomics and genomics, we demonstrated that autophagic activity is enhanced with age in *M. myotis* and *P. kuhlii* bats and uncovered genes under selective pressure that may be responsible for this upregulation.

MATERIALS AND METHODS

Comparative transcriptomic analyses of autophagy-associated genes between bat, human and mouse

Previous work from our group [9] suggested that autophagy-related pathways exhibit positive correlation with age in *M. myotis* bats, after correction for sampling site, year of recapture, sequencing bias and individual

variation. Seventy genes, which were enriched in the parental GO term 'autophagy', were in the module that was positively correlated with age in *M. myotis* bats (FDR < 0.05). To ascertain whether an increase in autophagy-related pathways over age was uniquely seen in bats, here we compared the age-related expression of these 70 autophagy-associated genes across bats, humans and mice using the Huang et al. data sets. The Spearman's rank correlation coefficients between gene expression and age across taxa were collated (Supplementary Table 6). To investigate the expression pattern at the pathway level, we employed the median of Spearman's rank correlation coefficients of all 70 genes enriched for the five autophagy related GO terms under the parental term 'autophagy' to ascertain their overall pathway expression pattern with age.

Animals and sampling

All sampling was carried out in accordance with the ethical guidelines in each country (see Supplementary Table 7). The captured individuals were healthy, not showing visible signs of sickness or infection. Wing biopsies were taken from *M. myotis* and *P. kuhlii* wild individuals using a 3 mm biopsy punch (2 per individual). Small clippings (approx. 3 mm wide) were taken from mice ears (C57BL/6J strain) (Supplementary Table 7). All the materials were stored at 4° C in cell culture growth medium (Dulbecco's MEM high glucose with stabilized glutamine, Biochrom/Merck, 20% FBS, Gibco) supplemented with 1% antibiotics mix (Penicillin-Streptomycin-Fungizone, Lonza BioWhittaker™), and delivered to the lab within 4 days. For the species included in the study, the maximum recorded life span (AnAge), source and age range are detailed in Supplementary Table 7. For each species, the longevity quotient (LQ, observed longevity / expected longevity [49]) was calculated, where expected longevity was obtained using a linear regression fitted to logged values of maximum longevity and mass for all non-flying eutherian species (slope = 0.186, intercept = 0.546) described by Foley et al. [5]. Age described as *n*+ indicates individuals first fitted with transponders as adults *n* years before the subsequent recapture, therefore the true age is unknown. The *n*+ individuals were only included in the oldest age groups (5+ for *M. myotis*, 5+ *for P. kuhlii*) and their age used as *n*+1 for the analyses. Additionally, NHEJ mice flank-skin derived primary fibroblasts were included ([19], Supplementary Table 7).

Establishment of primary fibroblasts

Primary skin fibroblasts were grown as previously described with some modifications [5]. Wing membrane (bats) and ear (mouse) skin samples were rinsed in fresh growth medium and minced into ~0.5 mm fragments using sterile blade. Skin fragments were resuspended in 3 cm cell culture treated Petri dishes in growth medium supplemented with 0.1 % collagenase type II. After overnight incubation at 37° C, 5% CO_2, the collagenase was replaced with fresh growth medium. Cells were then fed every 2 – 3 days with growth medium of reduced antibiotic concentration (0.2%). First fibroblast growth was observed after 3 days, and large fibroblast growth halos around fragments of tissue starting to approach one another were obtained after approximately 9-10 days. Typically, cells were passaged using trypsin-EDTA (0.025%) after 10 days of growth and seeded at 100k cells/well in 24-well plates. 24 hrs later, when 80-90% confluent, they were used for experiments.

Autophagy inducing treatments

Autophagy was induced by 5 hrs of serum deprivation. Where indicated, starvation treatment was performed in the presence of 100 nM bafilomycin A1 (Sigma-Aldrich) to block the autophagosome degradation. Alternatively, autophagy was induced by 5 hrs incubation with 5 µM rapamycin (Cayman Chemical). Following the treatments, cells were washed twice with ice cold PBS and lysed directly in the culture dishes with 55 µl of ice-cold RIPA buffer (20 mM Tris-HCl, pH 7.5; 150 mM NaCl; 1 mM Na2EDTA; 1 mM EGTA; 1% NP-40). After 5 min incubation on ice, the cells were stored at -80° C until western blot analysis.

Western blot

Total cell lysates were thawed at room temperature for 5 min, transferred to 1.5 ml tubes and mixed with cOmplete™, Mini, EDTA-free protease inhibitor cocktail (Roche) prior to centrifugation for 5 min, 13,000g. The supernatants were mixed 5x Laemmli buffer and a denaturing agent (Fermentas) and run on pre-cast 8-16% polyacrylamide gels (Biorad). Samples were transferred onto PVDF membrane (Biorad), blocked for 1 hr using 2 % non-fat milk in Tris-glycine buffer with 0.1% Tween (TGT), and then incubated overnight with LC3B primary antibody (Cell Signaling #2775) at a 1:500 dilution. The membranes were washed in TGT 3 times and then incubated with goat anti–rabbit secondary antibody (Invitrogen, #65-6120) for 1 hour at a 1:2000 dilution. Following 3 more washes, chemiluminescent detection was carried out using the Western Lightning Plus ECL substrate (PerkinElmer) and images were acquired with the LAS-4000 Image Analyzer (Fujifilm). The membrane was then washed in TGT buffer and then incubated for 1 hour with a GAPDH primary antibody (Cambridge Bioscience #3777R-100). Densitometric analyses of LC3II/I and

LC3/GAPDH signal were performed using ImageJ software [50], typically using images taken after 120 s exposure for LC3 staining and 30 s for GAPDH staining. Background subtraction option was used to process images prior to analysis, with options of sliding paraboloid and disabled smoothing. Statistical analyses of the results were performed using SPSS software.

P. kuhlii transcriptome assembly and annotation

Due to lack of genetic resources available for *P. kuhlii* (no genome available at time of analyses and experimentation), we used a transcriptome-based approach to obtain the coding sequences for *P. kuhlii*, required for further phylogenomic analyses. For fibroblast RNA-Seq library preparation, 200k cells/well were seeded in 12-well plates. 24 hrs later, when 80-90% confluent, serum deprivation treatment was performed for 12 hrs. High quality total RNA (RIN scores 9.3-10, 28S/18S 1.9-2.6) was extracted using RNeasy Mini Kit (Qiagen), and DNAse treated with TURBO DNA-free kit (Ambion) according to manufacturers' instructions. Oligo(dT)s were used to isolate mRNA as part of RNA-Seq library preparation. Paired-end sequencing was performed using the Illumina HiSeq2500 platform (Fasteris) resulting in on average 49.5 million paired-end reads (125 bp) per sample. Raw reads were scanned for adaptor sequences using 'fastq-mcf' from the ea-utils package [51]. A minimum base quality score of 25 and a length of 50bp were applied as filtering thresholds across each read. *De novo* assembly methodologies were used to generate the *P. kuhlii* transcriptome assembly [52]. *De novo* assemblies for each sample (3 control and 3 serum starved samples), in addition to a 'pooled' super assembly, were generated using Trinity (v2.3.2, [53]). All Trinity outputs were assessed for completeness using Benchmarking Universal Single-Copy Orthologs (BUSCO, [54]) and mammalian orthologs identified in OrthoDB (v9.1; 50 taxa, 4104 BUSCOs, [55]). Coding sequence regions in each assembled transcriptome were identified using FrameDP [56], with predicted peptide sequences less than 20 amino acids removed. Redundant transcripts (100% identical) were identified and removed using cd-hit-est [57], and the transcriptome completeness was further assessed using BUSCO. Blastx [58] was used to map all assembled transcripts to both the TrEMBL and UniProt [59], using an E-value of $1e^{-10}$, a sequence identity of 80% and a sequence coverage of 70% as thresholds.

Phylogenomic analyses

Gene sequence data

Genes enriched in the parental GO term 'autophagy' were retrieved from *M. myotis* blood transcriptomes (Supplementary Table 6) and autophagy-associated genes were retrieved through a search of gene products associated with the input term "autophagy", filtered for mammalian genes-only, on the Gene Ontology Consortium open database AmiGO [22] (Supplementary Table 8). This yielded a total of 558 genes after removing redundant names representing the same gene and genes of unknown function. These were used to mine the RefSeq genome annotations [60] of 62 eutherian mammals, representing basal eutherian divergences, including 10 bat species (Supplementary Table 9), using the gene IDs and the CDS mining methodology described in Hughes and Teeling [61]. Genes that were annotated in only 50% or less taxa were excluded from downstream analyses. This operation reduced the number of candidate genes to 406. Assembled RNA transcripts of these target genes were identified in *P. kuhlii* using tblastx [58], with 95% amino acid identity and query genes from *Myotis lucifugus*, *Myotis brandtii* and *Myotis davidii* (all *Myotis* species genomes available in Genbank). Removing genes that were not detected in the *P. kuhlii* assembled transcriptome further reduced the final gene number to a total of 274 genes (Supplementary Table 10). Additional taxa whose genomes are highly fragmented and yet to be annotated were mined for target genes using the Hughes and Teeling [61] annotation workflow. This workflow utilizes MAKER [62] with a number of additional pre- and post- annotation steps to recover a gene's CDS in highly fragmented genome assemblies. As these data were expected to be of lower quality given that they were from low coverage, fragmented genomes, two separate datasets were created: RefSeq only and RefSeq + MAKER output. The RefSeq + MAKER set contained additional sequence data from the all available additional bat genomes (n=5) at the time of analyses (*Rhinolophus ferrumequinum*, *Eidolon helvum*, *Megaderma lyra*, *Pteronotus parnellii*, and a proprietary *Myotis myotis* genome), and three non-chiropteran taxa *Choloepus hoffmanni*, *Procavia capensis* and *Manis pentadactyla* (Supplementary Table 11).

Sequence alignment

All gene files were translated from nucleotide to amino acid sequences and aligned using the phylogeny-aware aligner PRANK [63] with 5 iterations. An in-house Perl script was used to remove poorly aligned regions via Gblocks [64], using the minimum number of sequences allowed for conserved and flank positions, with the output modified alignments subsequently converted into codon alignments. This script is made available on GitHub at https://github.com/batlabucd/GenomeMining. All alignments were converted to PHYLIP format for analyses with PAML [65].

Selection tests

To investigate if selection could be detected in a number of different genes, both the branch-site (positive selection; Model A vs Model A1) and Clade Model C (divergent selection; Clade Model vs M2a_Rel) tests in the PAML package 'CodeML' were applied to all alignments for a variety of different ancestral and species-specific lineages. The ancestral bat, ancestral vespertilionid bat, and ancestral *Myotis* bat were designated as foreground branches for calculating omega (ω) (Supplementary Figure 5). We also investigated the selection pressure acting on species-specific lineages: *P. kuhlii* given the quality and availability of transcriptome data and *M. musculus* to compare selection pressures across our experimental taxa. The species tree used in these analyses was created using Meredith et al. [66] for interordinal mammalian relationships, with Foley et al. [5] and Teeling et al. [67] used for bat phylogenies (Supplementary Figure 5). All selection tests were implemented using the Optimised High-throughput Snakemake Automisation of PAML (OHSNAP) pipeline [5]. OHSNAP allows the fully automated execution of a number of CodeML runs in parallel, using multiple models and foreground branches, and was used to run more than 9600 CodeML instances. Likelihood ratio tests (LRTs) were used to compare the fit of the likelihood values from the null and alternative models, with one degree of freedom and *p*-values calculated using a chi-squared distribution. False discovery rate (FDR) correction was applied to *p*-values for each foreground branch and underlying model of selection, with resulting *p*-values above a significance level of 0.05 considered. Sites containing a Bayes Empirical Bayes (BEB) score probability of more than 95% in alignments showing significant differences between null and alternative models were considered to be under selection. These alignments were subsequently visualized to confirm data quality to avoid poorly aligned regions being considered as evidence for selection. Only the genes that had significant signals of selection in both datasets (RefSeq and RefSeq+MAKER) were reported. All steps involved in the phylogenomic analyses are summarized in Supplementary Figure 4. Instances of positive selection in the *P. kuhlii* lineage were further validated against recently published chromosome level genome assemblies made available through the Bat1K project [37].

Protein-protein interaction network analysis

The interactions between gene products highlighted by cell culture, transcriptomic, phylogenomic analyses in this study were evaluated with the Search Tool for the Retrieval of Interacting Genes/Proteins database, STRING, v.10.5 [23].

Data availability statement

The *P. kuhlii* fibroblasts transcriptomes generated as part of this analysis will be openly available through the National Center for Biotechnology Information Sequence Reads Archive under accession numbers SRR10129696 - SRR10129701 (BioProject ID: PRJNA565655). All generated nucleotide, protein and codon alignments for autophagy-associated genes under investigation are openly available from: https://figshare.com/s/96e220aba1b424671f5a.

AUTHOR CONTRIBUTIONS

J.K., A.G.L and E.C.T. conceived the project. The wild bat populations were sampled by A.G.L. (*P. kuhlii*) and Z.H. and E.C.T. (*M. myotis*). The bat and mouse fibroblast cells were grown and treated by J.K. western blot analysis of LC3 was performed by A.G.L. and J.K. C.S. and G.S.S. provided assistance with design and optimization of western blot experiments. V.G. provided the NHEJ samples. J.K. prepared samples for *P. kuhlii* transcriptome sequencing, and G.M.H, Z.H. and M.C. analysed the resulting data. Z.H. analysed the aging *Myotis* transcriptome data. G.M.H., J.K., A.G.L. and E.C.T. designed the phylogenomic selection tests. G.M.H. performed all selection tests. J.K. performed protein interaction network analysis. J.K, E.T., G.H., A.G.L. wrote the paper with the assistance of all authors.

ACKNOWLEDGMENTS

We acknowledge and thank the members of Bretagne Vivante, Eric Petit, Frédéric Touzalin, Sébastien Puechmaille, local volunteers and students from University College Dublin for their extensive help in sample collection and the owners/local authorities for allowing access to the French sites. We thank Roberto Toffoli and Paola Culasso for their help in sample collections. We thank Primož Presetnik, Ana Čehovin, Jasmina Kotnik, Tea Knapič, Lea Likozar, Eva Pavlovič, Monika Podgorelec, Janez Prešern and Roberta Rota for extensive help in the field captures in Slovenia. We thank Luke O'Neill (School of Biochemistry and Immunology, Trinity College Dublin) and Irina and Michael Conboy (Department of Bioengineering, Berkeley Research, University of California) for mouse ear samples. We acknowledge the Irish Centre for High-End Computing (ICHEC) for the provision of computational facilities and support. We thank Dr Sarah McLoughlin for critically reading the manuscript.

CONFLICTS OF INTEREST

The authors declare that they have no conflicts of interest.

FUNDING

This project was funded by a European Research Council Research Grant (ERC-2012-StG311000) awarded to E.C.T., a UCD Wellcome Institutional Strategic Support Fund, financed jointly by University College Dublin and SFI-HRB-Wellcome Biomedical Research Partnership (ref 204844/Z/16/Z) to E.C.T., an Irish Research Council Consolidator Laureate Award to E.C.T., a UCD School of Biology studentship to A.L. The French field work was supported by a Contrat Nature Grant awarded to Bretagne Vivante. V.G. is supported by grants from US National Institutes of Health.

REFERENCES

1. de Magalhães JP. The scientific quest for lasting youth: prospects for curing aging. Rejuvenation Res. 2014; 17:458–67. https://doi.org/10.1089/rej.2014.1580 PMID:25132068

2. Salmon AB, Leonard S, Masamsetti V, Pierce A, Podlutsky AJ, Podlutskaya N, Richardson A, Austad SN, Chaudhuri AR. The long lifespan of two bat species is correlated with resistance to protein oxidation and enhanced protein homeostasis. FASEB J. 2009; 23:2317–26. https://doi.org/10.1096/fj.08-122523 PMID:19244163

3. de Magalhães JP, Kean M. Endless paces of degeneration—applying comparative genomics to study evolution's moulding of longevity. EMBO Rep. 2013; 14:661–62. https://doi.org/10.1038/embor.2013.96 PMID:23846314

4. Austad SN. Methusaleh's zoo: How nature provides us with clues for extending human health span. J Comp Pathol. 2010 (Suppl 1); 142:S10–21. https://doi.org/10.1016/j.jcpa.2009.10.024 PMID:19962715

5. Foley NM, Hughes GM, Huang Z, Clarke M, Jebb D, Whelan CV, Petit EJ, Touzalin F, Farcy O, Jones G, Ransome RD, Kacprzyk J, O'Connell MJ, et al. Growing old, yet staying young: the role of telomeres in bats' exceptional longevity. Sci Adv. 2018; 4:eaao0926. https://doi.org/10.1126/sciadv.aao0926 PMID:29441358

6. Jebb D, Foley NM, Whelan CV, Touzalin F, Puechmaille SJ, Teeling EC. Population level mitogenomics of long-lived bats reveals dynamic heteroplasmy and challenges the free radical theory of ageing. Sci Rep. 2018; 8:13634. https://doi.org/10.1038/s41598-018-31093-2 PMID:30206380

7. Hughes GM, Leech J, Puechmaille SJ, Lopez JV, Teeling EC. Is there a link between aging and microbiome diversity in exceptional mammalian longevity? PeerJ. 2018; 6:e4174. https://doi.org/10.7717/peerj.4174 PMID:29333342

8. Ball HC, Levari-Shariati S, Cooper LN, Aliani M. Comparative metabolomics of aging in a long-lived bat: insights into the physiology of extreme longevity. PLoS One. 2018; 13:e0196154. https://doi.org/10.1371/journal.pone.0196154 PMID:29715267

9. Huang Z, Whelan CV, Foley NM, Jebb D, Touzalin F, Petit EJ, Puechmaille SJ, Teeling EC. Longitudinal comparative transcriptomics reveals unique mechanisms underlying extended healthspan in bats. Nat Ecol Evol. 2019; 3:1110–20. https://doi.org/10.1038/s41559-019-0913-3 PMID:31182815

10. Kaushik S, Cuervo AM. Proteostasis and aging. Nat Med. 2015; 21:1406–15. https://doi.org/10.1038/nm.4001 PMID:26646497

11. Muntané G, Farré X, Rodríguez JA, Pegueroles C, Hughes DA, de Magalhães JP, Gabaldón T, Navarro A. Biological processes modulating longevity across primates: A phylogenetic genome-phenome analysis. Mol Biol Evol. 2018; 35:1990–2004. https://doi.org/10.1093/molbev/msy105 PMID:29788292

12. Pride H, Yu Z, Sunchu B, Mochnick J, Coles A, Zhang Y, Buffenstein R, Hornsby PJ, Austad SN, Pérez VI. Long-lived species have improved proteostasis compared to phylogenetically-related shorter-lived species. Biochem Biophys Res Commun. 2015; 457:669–75. https://doi.org/10.1016/j.bbrc.2015.01.046 PMID:25615820

13. Laing ED, Sterling SL, Weir DL, Beauregard CR, Smith IL, Larsen SE, Wang LF, Snow AL, Schaefer BC, Broder CC. Enhanced autophagy contributes to reduced viral infection in black flying fox cells. Viruses. 2019; 11:260. https://doi.org/10.3390/v11030260 PMID:30875748

14. Gorbunova V, Seluanov A, Kennedy BK. The world goes bats: living longer and tolerating viruses. Cell Metab. 2020; 32:31–43. https://doi.org/10.1016/j.cmet.2020.06.013 PMID:32640245

15. Nakamura S, Yoshimori T. Autophagy and longevity. Mol Cells. 2018; 41:65–72. https://doi.org/10.14348/molcells.2018.2333 PMID:29370695

16. Madeo F, Zimmermann A, Maiuri MC, Kroemer G. Essential role for autophagy in life span extension. J Clin Invest. 2015; 125:85–93. https://doi.org/10.1172/JCI73946 PMID:25654554

17. Hansen M, Rubinsztein DC, Walker DW. Publisher correction: Autophagy as a promoter of longevity: insights from model organisms. Nat Rev Mol Cell Biol. 2018; 19:611. https://doi.org/10.1038/s41580-018-0048-4 PMID:30046055

18. Kim YC, Guan KL. mTOR: A pharmacologic target for autophagy regulation. J Clin Invest. 2015; 125:25–32. https://doi.org/10.1172/JCI73939 PMID:25654547

19. Vaidya A, Mao Z, Tian X, Spencer B, Seluanov A, Gorbunova V. Knock-in reporter mice demonstrate that DNA repair by non-homologous end joining declines with age. PLoS Genet. 2014; 10:e1004511. https://doi.org/10.1371/journal.pgen.1004511 PMID:25033455

20. Mizushima N, Yoshimori T. How to interpret LC3 immunoblotting. Autophagy. 2007; 3:542–45. https://doi.org/10.4161/auto.4600 PMID:17611390

21. Yamamoto A, Tagawa Y, Yoshimori T, Moriyama Y, Masaki R, Tashiro Y. Bafilomycin A1 prevents maturation of autophagic vacuoles by inhibiting fusion between autophagosomes and lysosomes in rat hepatoma cell line, H-4-II-E cells. Cell Struct Funct. 1998; 23:33–42. https://doi.org/10.1247/csf.23.33 PMID:9639028

22. Carbon S, Ireland A, Mungall CJ, Shu S, Marshall B, Lewis S, AmiGO Hub, and Web Presence Working Group. AmiGO: online access to ontology and annotation data. Bioinformatics. 2009; 25:288–89. https://doi.org/10.1093/bioinformatics/btn615 PMID:19033274

23. Szklarczyk D, Franceschini A, Wyder S, Forslund K, Heller D, Huerta-Cepas J, Simonovic M, Roth A, Santos A, Tsafou KP, Kuhn M, Bork P, Jensen LJ, von Mering C. STRING v10: protein-protein interaction networks, integrated over the tree of life. Nucleic Acids Res. 2015; 43:D447–52. https://doi.org/10.1093/nar/gku1003 PMID:25352553

24. Kroemer G. Autophagy: A druggable process that is deregulated in aging and human disease. J Clin Invest. 2015; 125:1–4. https://doi.org/10.1172/JCI78652 PMID:25654544

25. Liang CC, Wang C, Peng X, Gan B, Guan JL. Neural-specific deletion of FIP200 leads to cerebellar degeneration caused by increased neuronal death and axon degeneration. J Biol Chem. 2010; 285:3499–509. https://doi.org/10.1074/jbc.M109.072389 PMID:19940130

26. Davies SE, Hallett PJ, Moens T, Smith G, Mangano E, Kim HT, Goldberg AL, Liu JL, Isacson O, Tofaris GK. Enhanced ubiquitin-dependent degradation by Nedd4 protects against α-synuclein accumulation and toxicity in animal models of Parkinson' disease. Neurobiol Dis. 2014; 64:79–87. https://doi.org/10.1016/j.nbd.2013.12.011 PMID:24388974

27. Ulgherait M, Rana A, Rera M, Graniel J, Walker DW. AMPK modulates tissue and organismal aging in a non-cell-autonomous manner. Cell Rep. 2014; 8:1767–80. https://doi.org/10.1016/j.celrep.2014.08.006 PMID:25199830

28. Satoh A, Brace CS, Rensing N, Cliften P, Wozniak DF, Herzog ED, Yamada KA, Imai S. Sirt1 extends life span and delays aging in mice through the regulation of Nk2 homeobox 1 in the DMH and LH. Cell Metab. 2013; 18:416–30. https://doi.org/10.1016/j.cmet.2013.07.013 PMID:24011076

29. Landis GN, Bhole D, Tower J. A search for doxycycline-dependent mutations that increase drosophila melanogaster life span identifies the VhaSFD, Sugar baby, filamin, fwd and Cctl genes. Genome Biol. 2003; 4:R8. https://doi.org/10.1186/gb-2003-4-2-r8 PMID:12620118

30. Rana A, Oliveira MP, Khamoui AV, Aparicio R, Rera M, Rossiter HB, Walker DW. Promoting Drp1-mediated mitochondrial fission in midlife prolongs healthy lifespan of drosophila melanogaster. Nat Commun. 2017; 8:448. https://doi.org/10.1038/s41467-017-00525-4 PMID:28878259

31. Rubinsztein DC, Mariño G, Kroemer G. Autophagy and aging. Cell. 2011; 146:682–95. https://doi.org/10.1016/j.cell.2011.07.030 PMID:21884931

32. Kunstyr I, Leuenberger HG. Gerontological data of C57BL/6J mice. I. Sex differences in survival curves. J Gerontol. 1975; 30:157–62. https://doi.org/10.1093/geronj/30.2.157 PMID:1123533

33. Kim HS, Park SY, Moon SH, Lee JD, Kim S. Autophagy in human skin fibroblasts: impact of age. Int J Mol Sci. 2018; 19:2254.

https://doi.org/10.3390/ijms19082254
PMID:30071626

34. Omata Y, Lim YM, Akao Y, Tsuda L. Age-induced reduction of autophagy-related gene expression is associated with onset of Alzheimer's disease. Am J Neurodegener Dis. 2014; 3:134–42.
PMID:25628964

35. Kacprzyk J, Hughes GM, Palsson-McDermott EM, Quinn SR, Puechmaille SJ, O'Neill LAJ, Teeling EC. A potent anti-inflammatory response in bat macrophages may be linked to extended longevity and viral tolerance. Acta Chiropt. 2017; 19:219–28.
https://doi.org/10.3161/15081109ACC2017.19.2.001

36. Munshi-South J, Wilkinson GS. Bats and birds: exceptional longevity despite high metabolic rates. Ageing Res Rev. 2010; 9:12–19.
https://doi.org/10.1016/j.arr.2009.07.006
PMID:19643206

37. Jebb D, Huang Z, Pippel M, Hughes GM, Lavrichenko K, Devanna P, Winkler S, Jermiin LS, Skirmuntt EC, Katzourakis A, Burkitt-Gray L, Ray DA, Sullivan KA, et al. Six reference-quality genomes reveal evolution of bat adaptations. Nature. 2020; 583:578–84.
https://doi.org/10.1038/s41586-020-2486-3
PMID:32699395

38. Rubinsztein DC, Codogno P, Levine B. Autophagy modulation as a potential therapeutic target for diverse diseases. Nat Rev Drug Discov. 2012; 11:709–30.
https://doi.org/10.1038/nrd3802 PMID:22935804

39. Wang N, Tan HY, Li S, Feng Y. Atg9b deficiency suppresses autophagy and potentiates endoplasmic reticulum stress-associated hepatocyte apoptosis in hepatocarcinogenesis. Theranostics. 2017; 7:2325–38.
https://doi.org/10.7150/thno.18225 PMID:28740555

40. Mura M, Hopkins TG, Michael T, Abd-Latip N, Weir J, Aboagye E, Mauri F, Jameson C, Sturge J, Gabra H, Bushell M, Willis AE, Curry E, Blagden SP. LARP1 post-transcriptionally regulates mTOR and contributes to cancer progression. Oncogene. 2015; 34:5025–36.
https://doi.org/10.1038/onc.2014.428
PMID:25531318

41. Pan H, Finkel T. Key proteins and pathways that regulate lifespan. J Biol Chem. 2017; 292:6452–60.
https://doi.org/10.1074/jbc.R116.771915
PMID:28264931

42. Bagshaw RD, Mahuran DJ, Callahan JW. Lysosomal membrane proteomics and biogenesis of lysosomes. Mol Neurobiol. 2005; 32:27–41.
https://doi.org/10.1385/MN:32:1:027
PMID:16077181

43. Takahashi Y, He H, Tang Z, Hattori T, Liu Y, Young MM, Serfass JM, Chen L, Gebru M, Chen C, Wills CA, Atkinson JM, Chen H, et al. An autophagy assay reveals the ESCRT-III component CHMP2A as a regulator of phagophore closure. Nat Commun. 2018; 9:2855.
https://doi.org/10.1038/s41467-018-05254-w
PMID:30030437

44. Ma S, Upneja A, Galecki A, Tsai YM, Burant CF, Raskind S, Zhang Q, Zhang ZD, Seluanov A, Gorbunova V, Clish CB, Miller RA, Gladyshev VN. Cell culture-based profiling across mammals reveals DNA repair and metabolism as determinants of species longevity. Elife. 2016; 5:e19130.
https://doi.org/10.7554/eLife.19130 PMID:27874830

45. Hailey DW, Rambold AS, Satpute-Krishnan P, Mitra K, Sougrat R, Kim PK, Lippincott-Schwartz J. Mitochondria supply membranes for autophagosome biogenesis during starvation. Cell. 2010; 141:656–67.
https://doi.org/10.1016/j.cell.2010.04.009
PMID:20478256

46. Sebastián D, Sorianello E, Segalés J, Irazoki A, Ruiz-Bonilla V, Sala D, Planet E, Berenguer-Llergo A, Muñoz JP, Sánchez-Feutrie M, Plana N, Hernández-Álvarez MI, Serrano AL, et al. Mfn2 deficiency links age-related sarcopenia and impaired autophagy to activation of an adaptive mitophagy pathway. EMBO J. 2016; 35:1677–93.
https://doi.org/10.15252/embj.201593084
PMID:27334614

47. Wang P, Kou D, Le W. Roles of VMP1 in autophagy and ER-membrane contact: potential implications in neurodegenerative disorders. Front Mol Neurosci. 2020; 13:42.
https://doi.org/10.3389/fnmol.2020.00042
PMID:32296305

48. Dmitrieva VG, Zuikova EB, Nosova EV, Limborska SA, Dergunova LV, Savushikin EV, Litvinov DY, Dergunov AD. Key human blood cells genes involved in artherogenesis and metabolism of high density lipoproteins. Mol Genet Microbiol Virol. 2018; 33:84–90.
https://doi.org/10.3103/S0891416818020064

49. Austad SN, Fischer KE. Mammalian aging, metabolism, and ecology: evidence from the bats and marsupials. J Gerontol. 1991; 46:B47–53.
https://doi.org/10.1093/geronj/46.2.b47
PMID:1997563

50. Schneider CA, Rasband WS, Eliceiri KW. NIH image to ImageJ: 25 years of image analysis. Nat Methods. 2012; 9:671–75.
https://doi.org/10.1038/nmeth.2089
PMID:22930834

51. Aronesty E. ea-utils: Command-line tools for processing biological sequencing data. 2011.

52. Huang Z, Jebb D, Teeling EC. Blood miRNomes and transcriptomes reveal novel longevity mechanisms in the long-lived bat, myotis myotis. BMC Genomics. 2016; 17:906. https://doi.org/10.1186/s12864-016-3227-8 PMID:27832764

53. Haas BJ, Papanicolaou A, Yassour M, Grabherr M, Blood PD, Bowden J, Couger MB, Eccles D, Li B, Lieber M, MacManes MD, Ott M, Orvis J, et al. De novo transcript sequence reconstruction from RNA-seq using the trinity platform for reference generation and analysis. Nat Protoc. 2013; 8:1494–512. https://doi.org/10.1038/nprot.2013.084 PMID:23845962

54. Simão FA, Waterhouse RM, Ioannidis P, Kriventseva EV, Zdobnov EM. BUSCO: assessing genome assembly and annotation completeness with single-copy orthologs. Bioinformatics. 2015; 31:3210–12. https://doi.org/10.1093/bioinformatics/btv351 PMID:26059717

55. Zdobnov EM, Tegenfeldt F, Kuznetsov D, Waterhouse RM, Simão FA, Ioannidis P, Seppey M, Loetscher A, Kriventseva EV. OrthoDB v9.1: cataloging evolutionary and functional annotations for animal, fungal, plant, archaeal, bacterial and viral orthologs. Nucleic Acids Res. 2017; 45:D744–49. https://doi.org/10.1093/nar/gkw1119 PMID:27899580

56. Gouzy J, Carrere S, Schiex T. FrameDP: sensitive peptide detection on noisy matured sequences. Bioinformatics. 2009; 25:670–71. https://doi.org/10.1093/bioinformatics/btp024 PMID:19153134

57. Fu L, Niu B, Zhu Z, Wu S, Li W. CD-HIT: Accelerated for clustering the next-generation sequencing data. Bioinformatics. 2012; 28:3150–52. https://doi.org/10.1093/bioinformatics/bts565 PMID:23060610

58. Altschul SF, Madden TL, Schäffer AA, Zhang J, Zhang Z, Miller W, Lipman DJ. Gapped BLAST and PSI-BLAST: A new generation of protein database search programs. Nucleic Acids Res. 1997; 25:3389–402. https://doi.org/10.1093/nar/25.17.3389 PMID:9254694

59. The UniProt Consortium. UniProt: the universal protein knowledgebase. Nucleic Acids Res. 2017; 45:D158–69. https://doi.org/10.1093/nar/gkw1099 PMID:27899622

60. O'Leary NA, Wright MW, Brister JR, Ciufo S, Haddad D, McVeigh R, Rajput B, Robbertse B, Smith-White B, Ako-Adjei D, Astashyn A, Badretdin A, Bao Y, et al. Reference sequence (RefSeq) database at NCBI: current status, taxonomic expansion, and functional annotation. Nucleic Acids Res. 2016; 44:D733–45. https://doi.org/10.1093/nar/gkv1189 PMID:26553804

61. Hughes GM, Teeling EC. AGILE: An assembled genome mining pipeline. Bioinformatics. 2019; 35:1252–54. https://doi.org/10.1093/bioinformatics/bty781 PMID:30184049

62. Cantarel BL, Korf I, Robb SM, Parra G, Ross E, Moore B, Holt C, Sánchez Alvarado A, Yandell M. MAKER: An easy-to-use annotation pipeline designed for emerging model organism genomes. Genome Res. 2008; 18:188–96. https://doi.org/10.1101/gr.6743907 PMID:18025269

63. Löytynoja A, Goldman N. Phylogeny-aware gap placement prevents errors in sequence alignment and evolutionary analysis. Science. 2008; 320:1632–35. https://doi.org/10.1126/science.1158395 PMID:18566285

64. Castresana J. Selection of conserved blocks from multiple alignments for their use in phylogenetic analysis. Mol Biol Evol. 2000; 17:540–52. https://doi.org/10.1093/oxfordjournals.molbev.a026334 PMID:10742046

65. Yang Z. PAML 4: phylogenetic analysis by maximum likelihood. Mol Biol Evol. 2007; 24:1586–91. https://doi.org/10.1093/molbev/msm088 PMID:17483113

66. Meredith RW, Janečka JE, Gatesy J, Ryder OA, Fisher CA, Teeling EC, Goodbla A, Eizirik E, Simão TL, Stadler T, Rabosky DL, Honeycutt RL, Flynn JJ, et al. Impacts of the cretaceous terrestrial revolution and KPg extinction on mammal diversification. Science. 2011; 334:521–24. https://doi.org/10.1126/science.1211028 PMID:21940861

67. Teeling EC, Vernes SC, Dávalos LM, Ray DA, Gilbert MT, Myers E, and Bat1K Consortium. Bat biology, genomes, and the Bat1K project: to generate chromosome-level genomes for all living bat species. Annu Rev Anim Biosci. 2018; 6:23–46. https://doi.org/10.1146/annurev-animal-022516-022811 PMID:29166127

SUPPLEMENTARY MATERIALS

Analysis of starvation-induced differential gene expression of autophagy-associated genes

The *de novo* assembly generated from the pooled transcriptome (3 control and 3 serum starved samples, n=6) was used as a common reference for transcript quantification. For each sample, transcripts were quantified using Salmon (v0.9) [1] with the parameters - *IFS*. Due to higher sensitivity and accuracy, only the protein-coding genes with known functions in the gene-level analysis were investigated. To achieve this, transcripts with the same gene annotation were regarded as different transcripts of the same gene, and their abundance estimates were, accordingly, aggregated to the gene-level using the Bioconductor R package *tximport* [2]. This formed a gene expression matrix, with the horizontal axis representing all 6 samples and the vertical axis representing protein-coding genes. Autophagy-associated genes were identified through a search of gene products associated with the input term "autophagy" on the Gene Ontology Consortium open database AmiGO [3] and by removing redundant names representing the same gene and genes of unknown function. The differential expression analysis of these genes induced by serum starvation was performed using *DESeq2* [4]. The genes with a False Discovery Rate (FDR) < 0.05 were considered significantly differentially expressed (Supplementary Table 2).

REFERENCES

1. Patro R, Duggal G, Love MI, Irizarry RA, Kingsford C. Salmon provides fast and bias-aware quantification of transcript expression. Nat Methods. 2017; 14:417–19. https://doi.org/10.1038/nmeth.4197 PMID:28263959

2. Soneson C, Love MI, Robinson MD. Differential analyses for RNA-seq: transcript-level estimates improve gene-level inferences. F1000Res. 2015; 4:1521. https://doi.org/10.12688/f1000research.7563.2 PMID:26925227

3. Carbon S, Ireland A, Mungall CJ, Shu S, Marshall B, Lewis S; AmiGO Hub; Web Presence Working Group. AmiGO: online access to ontology and annotation data. Bioinformatics. 2009; 25:288–89. https://doi.org/10.1093/bioinformatics/btn615 PMID:19033274

4. Love MI, Huber W, Anders S. Moderated estimation of fold change and dispersion for RNA-seq data with DESeq2. Genome Biol. 2014; 15:550. https://doi.org/10.1186/s13059-014-0550-8 PMID:25516281

Supplementary Figures

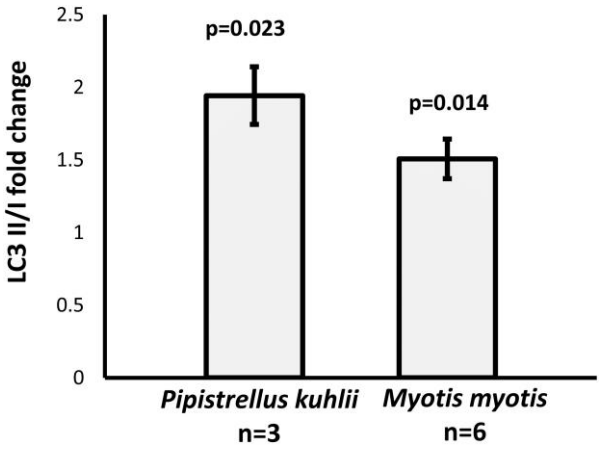

Supplementary Figure 1. Rapamycin-induced change in LC3 II/I ratio in skin-derived fibroblasts from *P. kuhlii* and M. myotis. Data represent mean fold change of LC3 II/I ratio induced by 5μM rapamycin treatment ±SEM (p-values: two-tailed t-test). Individuals tested were 0-3 years old (*P. kuhlii*) and 0-2 years old (*M. myotis*).

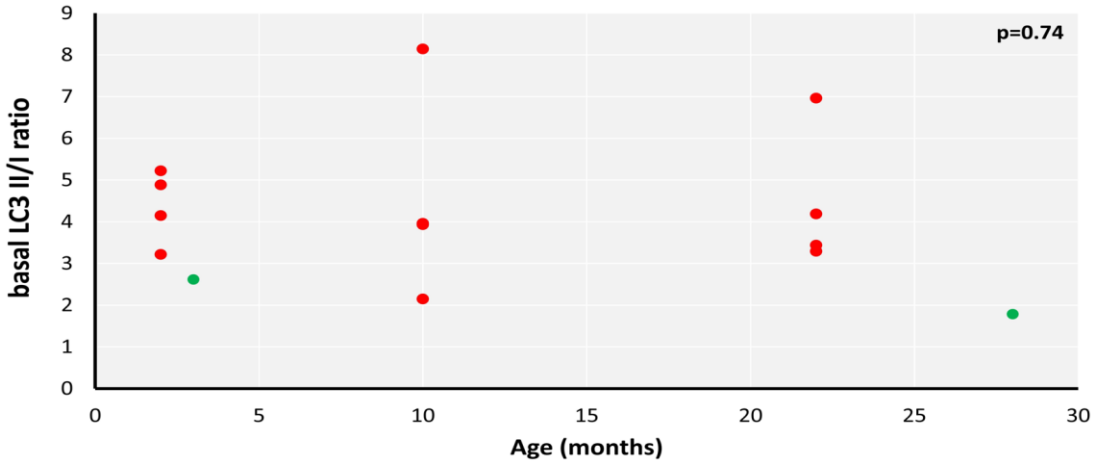

Supplementary Figure 2. Basal LC3 II/I ratio does not increase with age in mouse. In addition to mouse fibroblasts isolated from mouse ear (n=14, red dots), we included the flank skin derived fibroblasts from homozygous NHEJ mouse generated by Vaidya et al., (2014) (n=2, green dots). The LC3II/I ratio was determined as described in experimental procedures and p-value in the top right-hand corner of the plot indicate the significance of linear model.

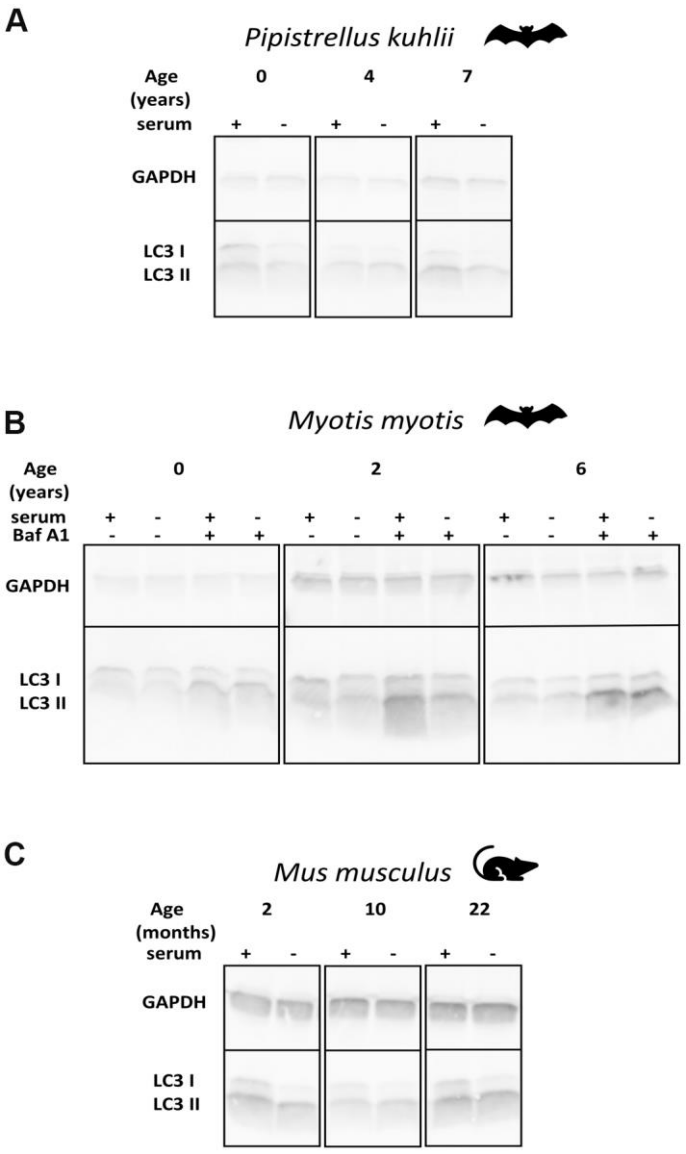

Supplementary Figure 3. Representative western blot gels for GAPDH and LC3II/LC3I per each species. (**A**) *P. kuhlii*, (**B**) *M. myotis* and (**C**) *M. musculus*.

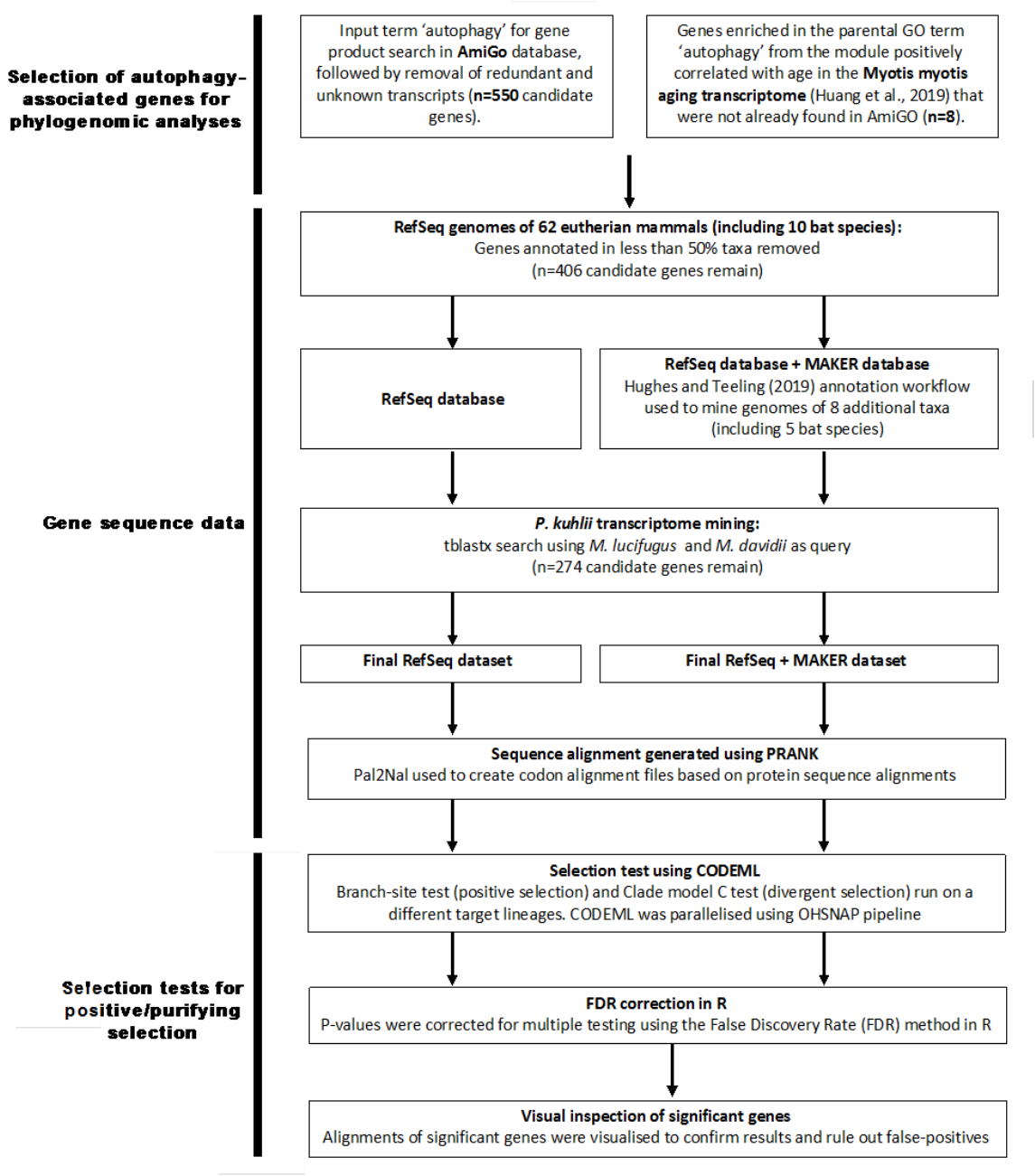

Supplementary Figure 4. Roadmap for phylogenomic analyses performed on autophagy-associated genes across eutherian mammals.

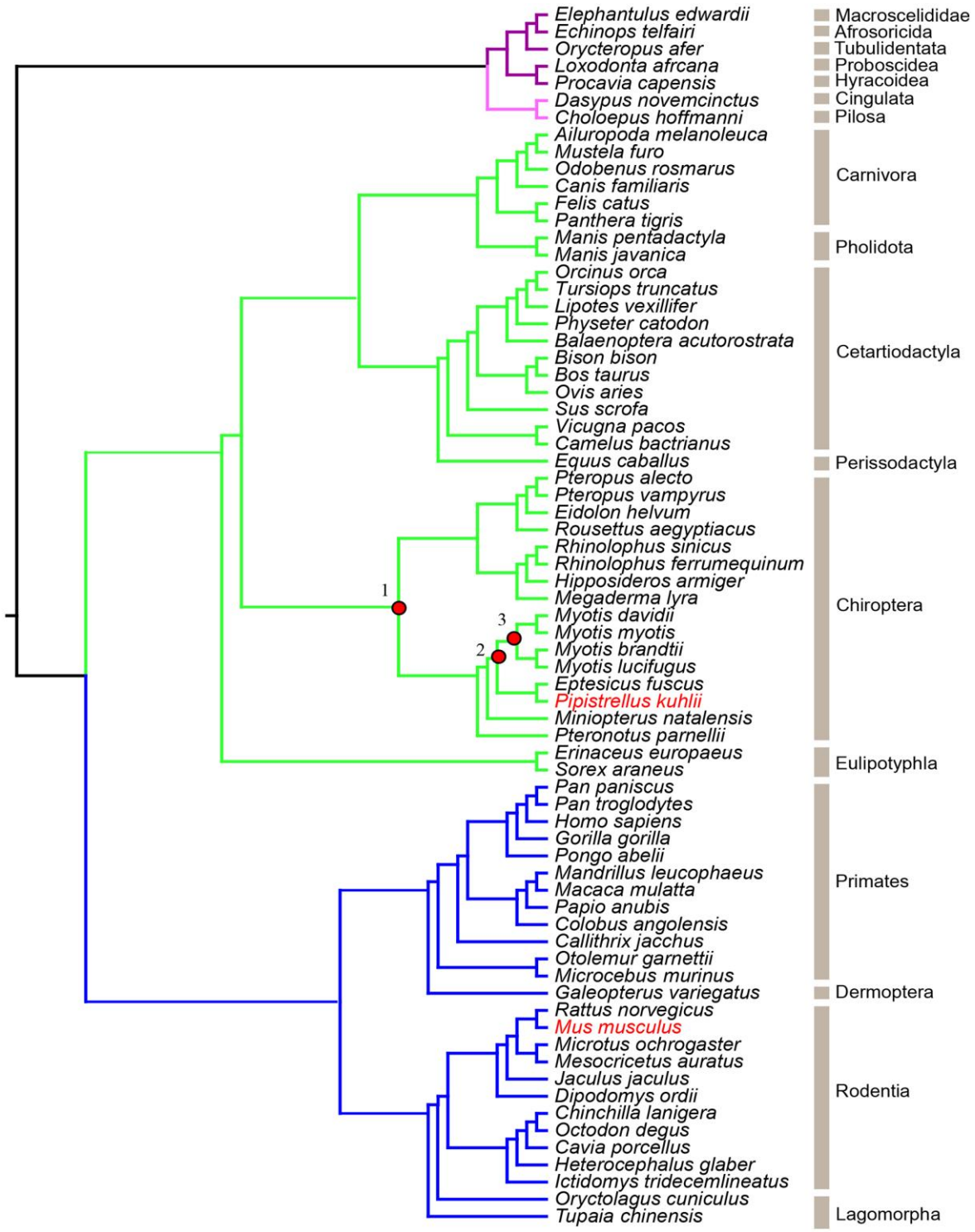

Supplementary Figure 5. Mammalian species tree. Patterns of selection were investigated for in a number of different ancestral bats branches (ancestral bat, ancestral *Vespertilionidae* and ancestral *Myotis* branches, labelled node 1, 2 and 3, respectively) and individual lineages (*P. kuhlii, M. musculus* and *M. myotis,* highlighted in red). This was done using autophagy-related gene sequences mined from mammalian genomes across all eutherian orders.

Supplementary Tables

Please browse Full Text version to see the data of Supplementary Tables 2, 4, 8, 10.

Supplementary Table 1A. Transcriptome read data.

Sample	Status	Number of reads	Number of reads trimmed
Individual 1	Control	49,387,054	12,904,046
Individual 2	Control	52,629,254	15,320,180
Individual 3	Control	48,344,678	13,888,881
Total	**Control**	**150,360,986**	**42,113,107**
Individual 1	Starved	57,071,722	12,688,612
Individual 2	Starved	47,388,124	13,039,158
Individual 3	Starved	42,244,472	11,607,783
Total	**Starved**	**146,704,318**	**37,335,553**
Abs. Total	-	297,065,304	79,448,660

Supplementary Table 1B. Transcriptome analyses.

Sample	Status	Trinity transcripts	BUSCO %	Complete BUSCOS
C13	Control	314,290	79.9	3276
C14	Control	294,959	79.4	3257
C16	Control	282,973	78.7	3232
Total		**892,222**	-	-
S13	Starved	312,523	78.8	3237
S14	Starved	315,358	78	3199
S16	Starved	269,709	77.9	3197
Total		**897,590**	-	-
Abs. Total	-	1,789,812	-	-
Pooled	-	681,843	84.2	3458
Final	-	271,767	83.6	3432

Supplementary Table 2. Differentially expressed (FDR<0.05) autophagy-related genes.

Supplementary Table 3. Codeml results.

Model	Gene	Dataset	Site(s) in alignment	Corresponding sites in amino acid sequence	FDR p-value	ω
Ancestral bat lineage						
Branch-site	*ATG9B*	RefSeq	60	60V (human: 59S)	0.009	Fg 443.74
		RefSeq + MAKER	60		0.004	Fg 434.69
Clade Model C	*MFN2*	RefSeq	-	-	0.002	Fg 3.38 Bg 0.19
		RefSeq + MAKER	-	-	0.035	Fg 2.35 Bg 0.20
***Vespertilionidae* ancestral lineage**						
Branch-site	*LARP1*	RefSeq	574	605N (human 684F)	0.008	Fg 58.87
		RefSeq + MAKER	546	605N (human 684F)	0.001	Fg 61.62
Clade Model C	*MTOR*	RefSeq	-	-	0.007	Fg 1.41 Bg 0.21
		RefSeq + MAKER	-	-	0.015	Fg 1.39 Bg 0.21
	NPC1	RefSeq	-	-	0.004	Fg 0.12 Bg 0.24
		RefSeq + MAKER	-	-	0.002	Fg 0.11 Bg 0.25
	STOM	RefSeq	-	-	0.0004	Fg 2.53 Bg 0.17
		RefSeq + MAKER	-	-	0.0006	Fg 2.41 Bg 0.18
	VPS4A	RefSeq	-	-	0.003	Fg 1.4 Bg 0.15
		RefSeq + MAKER	-	-	0.002	Fg 1.57 Bg 0.14
Pipistrellus kuhlli						
Branch-site	*VMP1*	RefSeq	No BEB sites	-	0.017	Fg: 999
		RefSeq + MAKER	170	170P (human 170D)	0.025	Fg: 999
	ZDHHC8	RefSeq	588	585A (human 591S)	0.017	Fg: 120.36
		RefSeq + MAKER	588, 754	585A (human 591S), 723R (human 760A)	0.026	Fg: 129.48
Clade Model C	*SFRP4*	RefSeq	-	-	0.003	Fg 1.29 Bg 0.21
		RefSeq + MAKER	-	-	0.003	Fg 1.32 Bg 0.21
Mus musculus						
Branch-site	*PSAP*	RefSeq	248, 471	251C (human 252A), 506G (human 476S)	0.001	Fg: 123.42
		RefSeq + MAKER	248, 468	251C (human 252A), 506G (human 476S)	0.006	Fg: 123.34

Clade Model C	*SNX14*	RefSeq	-	-	0.04	Fg 0.00 Bg 0.18
		RefSeq + MAKER	-	-	0.013	Fg 0.00 Bg 0.19

Fg = Foreground, Bg = Background. Bat lineage-specific sites under positive selection are reported with reference to corresponding amino acid in human CDS. Sites showing significant selection identified in optimized alignments and their corresponding amino acid position are shown.

Supplementary Table 4. Functional enrichment in biological process GO terms of the STRING protein-protein interaction network including genes under selective pressure in bat lineages, genes showing bat-specific upregulation with age, and LC3.

Supplementary Table 5. Functional enrichment in KEGG pathways of the STRING protein-protein interaction network including genes under selective pressure in bat lineages, genes showing bat-specific upregulation with age, and LC3.

Pathway ID	Pathway description	Observed gene count	FDR	Matching protein in the network
5169	Epstein-Barr virus infection	6	0.000128	Csnk2a1,Eif2ak4,Map3k7,Nedd4,Pik3ca,Tbk1
5162	Measles	5	0.000257	Csnk2a1,Eif2ak4,Map3k7,Pik3ca,Tbk1
4144	Endocytosis	5	0.00138	Nedd4,Sh3glb1,Vps36,Vps4a,Vta1
4140	Regulation of autophagy	3	0.00208	Pik3c3,Pik3r4,Ulk2
4152	AMPK signaling pathway	4	0.00211	Map3k7,Mtor,Pik3ca,Sirt1
4150	mTOR signaling pathway	3	0.00495	Mtor,Pik3ca,Ulk2
5168	Herpes simplex infection	4	0.00832	Csnk2a1,Eif2ak4,Map3k7,Tbk1
4620	Toll-like receptor signaling pathway	3	0.016	Map3k7,Pik3ca,Tbk1
4668	TNF signaling pathway	3	0.0178	Dnm1l,Map3k7,Pik3ca
5160	Hepatitis C	3	0.03	Eif2ak4,Pik3ca,Tbk1
5206	MicroRNAs in cancer	3	0.0303	Mtor,Rock1,Sirt1
4145	Phagosome	3	0.0424	Atp6v1c1,Atp6v1h,Pik3c3
5164	Influenza A	3	0.0442	Eif2ak4,Pik3ca,Tbk1
4930	Type II diabetes mellitus	2	0.0498	Mtor,Pik3ca

Supplementary Table 6. Genes enriched in the parental GO term 'autophagy' that showed correlation with age in M.

Gene	Bat	Human	Mouse
PIK3CA	0.483	-0.233	-0.568
ROCK1	0.468	-0.091	-0.41
RB1CC1	0.446	-0.143	-0.164
ATP6V1E2	0.438	-0.469	NA
RAB12	0.423	0.075	0.254
CSNK2A1	0.415	-0.015	-0.406
SCFD1	0.385	-0.235	0.027
NEDD4	0.383	-0.043	-0.1
UVRAG	0.36	0.156	0.087
POLR3A	0.343	0.17	-0.185
ATG3	0.341	-0.117	0.508
MTDH	0.318	-0.148	0.586
CISD2	0.314	0.079	0.28
PIK3CB	0.308	-0.14	0.497
ATG4C	0.296	-0.281	0.656
PAFAH1B2	0.293	-0.278	-0.097
MAPK8	0.286	0.099	-0.187
USP33	0.278	-0.237	-0.165
STAM	0.276	0.029	-0.213
FIS1	0.275	0.111	-0.032
MID2	0.274	0.218	0.262
TRAPPC8	0.274	-0.167	-0.066
ULK2	0.271	-0.017	-0.312
FBXW7	0.267	0.074	0.112
TOMM70	0.267	NA	NA
SIRT1	0.243	-0.091	-0.566
HERC1	0.241	0.06	0.086
VPS26A	0.24	0.046	0.367
PRKAB2	0.234	-0.157	0.551
STAM2	0.226	-0.299	0.334
SNX14	0.214	-0.27	-0.158
EP300	0.213	-0.17	0.013
VTA1	0.208	-0.302	-0.327
MAP3K7	0.203	-0.213	-0.247
TBC1D5	0.198	-0.231	0.111
TBK1	0.198	-0.218	-0.215
SNX5	0.19	0.143	-0.653
VPS36	0.179	-0.207	-0.483
NRBF2	0.177	-0.236	-0.361
WDFY3	0.176	-0.134	0.703
DNM1L	0.168	-0.081	-0.245
VTI1A	0.164	0.042	0.482
UBXN2B	0.146	-0.14	-0.179
EIF2AK4	0.141	-0.069	-0.361
WDR41	0.138	-0.121	0.275
RIPK2	0.137	0.232	-0.214

SH3GLB1	0.132	-0.149	-0.039
ATG4A	0.121	-0.063	0.094
PIK3R4	0.11	-0.227	-0.457
ATG5	0.108	-0.082	0.227
IFT88	0.104	-0.124	0.268
VIPAS39	0.103	-0.202	NA
ATP6V1H	0.099	-0.172	-0.032
SPTLC1	0.093	-0.2	0.072
PIK3C3	0.077	-0.268	-0.269
ATG10	0.076	-0.105	0.147
PTK2	0.061	0.109	0.484
RAB3GAP1	0.053	-0.013	-0.567
AMBRA1	0.052	0.153	-0.323
EPM2A	0.048	0.025	0.268
ANXA7	0.046	-0.2	0.383
ATP6V1C1	0.03	-0.186	-0.09
U2AF1	0.03	-0.053	-0.207
ATP6V0A1	0.021	0.015	0.181
RHEB	-0.006	-0.018	0.356
VPS4B	-0.023	-0.248	0.202
ACTL6A	-0.066	-0.327	-0.318
SREBF2	-0.074	-0.037	-0.03
TPCN1	-0.08	-0.151	0.112
MTMR3	-0.084	-0.012	0.067

myotis bats. The Spearman's rank correlation coefficients between their expression and age in bat, human and mouse were extracted from Huang et al. (2019). NA – transcript not detected in the blood transcriptome.

Supplementary Table 7. Taxonomic information: List of species included in the study, their record lifespan from AnAge, source of the samples, age ranges of individuals included in the study and sampling permit details.

Species	Max. lifespan	Source	Sample	Age range	Permit details for sampling wild bat populations
M. myotis	37.1yrs	Wild population, Brittany, France	wing punches	0 - 7+yrs	Arrêté préfectoral (18/07/2013 and 05/08/2013) issued to Eric Petit, Frédéric Touzalin and Sébastien Puechmaille by Préfet du Morbihan, valid between 15th June - 15th September; 2013-2017 inclusive
P. kuhlii	8yrs	Wild population, Krašnja, Slovenia Wild population, Piemonte, Italy	wing punches	0 – 7+ yrs	Aut. Prot. N°: 13040, issued to Roberto Toffoli and Andrea Locatelli by the Italian ministry for the territory and sea safeguard (Ministero della tutela del territorio e del mare) Aut N°: 35601-35/2010-6, issued to Primož Presetnik by the Slovenian Environment Agency (Agencija Republike Slovenije za okolje)
M. musculus (C57BL/6J strain)	4 yrs	Conboy laboratory (Department of Bioengineering, Berkeley Research, University of California) and O'Neill laboratory (School of Biochemistry and Immunology, Trinity College Dublin)	ear clippings	2 – 22 months	not applicable
M. musculus (NHEJ background)	na	Gorbanova laboratory (Departments of Biology and Medicine, University of Rochester, Rochester, NY 14627, USA)	flank-skin derived primary fibroblasts developed as decribed in Vaidya et al. (2014)	3 and 28 months	not applicable

Supplementary Table 8. List of genes involved in mammalian autophagy retrived from AmiGO database using search term 'autophagy'.

Supplementary Table 9. RefSeq mammals used.

Mammalian genome	Number of genes	Order
Loxodonta africana	244	Afrotheria
Elephantulus edwardii	232	Afrotheria
Echinops telfairi	254	Afrotheria
Orycteropus afer	262	Afrotheria
Dasypus novemcinctus	241	Xenarthra
Lipotes vexillifer	249	Cetartiodactyla
Orcinus orca	261	Cetartiodactyla
Tursiops truncatus	168	Cetartiodactyla
Physeter catodon	156	Cetartiodactyla
Balaenoptera acutorostrata	240	Cetartiodactyla
Bison bison	254	Cetartiodactyla
Bos Taurus	261	Cetartiodactyla
Ovis aries	213	Cetartiodactyla
Sus scrofa	228	Cetartiodactyla
Camelus bactrianus	252	Cetartiodactyla
Vicugna pacos	248	Cetartiodactyla
Equus caballus	249	Perissodactyla
Manis javanica	248	Pholidota
Felis catus	263	Carnivora
Panthera tigris	238	Carnivora
Ailuropoda melanoleuca	255	Carnivora
Mustela putorius	61	Carnivora
Odobenus rosmarus	247	Carnivora
Canis lupus	134	Carnivora
Pteropus alecto	250	Chiroptera
Pteropus vampyrus	258	Chiroptera
Rousettus aegyptiacus	250	Chiroptera
Rhinolophus sinicus	263	Chiroptera
Hipposideros armiger	240	Chiroptera
Miniopterus natalensis	256	Chiroptera
Eptesicus fuscus	261	Chiroptera
Myotis brandtii	257	Chiroptera
Myotis lucifugus	244	Chiroptera
Myotis davidii	254	Chiroptera
Erinaceus europaeus	252	Eulipotyphla
Sorex araneus	121	Eulipotyphla
Galeopterus variegatus	69	Dermoptera
Otolemur garnettii	260	Primates
Microcebus murinus	249	Primates
Callithrix jacchus	235	Primates
Colobus angolensis	211	Primates
Papio anubis	171	Primates
Mandrillus leucophaeus	236	Primates

Macaca mulatta	259	Primates
Pongo abelii	236	Primates
Gorilla gorilla	235	Primates
Homo sapiens	267	Primates
Pan paniscus	254	Primates
Pan troglodytes	246	Primates
Tupaia chinensis	247	Scandentia
Oryctolagus cuniculus	237	Lagomorpha
Microtus ochrogaster	260	Rodentia
Mesocricetus auratus	255	Rodentia
Rattus norvegicus	263	Rodentia
Mus musculus	264	Rodentia
Jaculus jaculus	261	Rodentia
Dipodomys ordii	264	Rodentia
Ictidomys tridecemlineatus	262	Rodentia
Chinchilla lanigera	258	Rodentia
Octodon degus	137	Rodentia
Cavia porcellus	255	Rodentia
Heterocephalus glaber	253	Rodentia

The mammals for which a RefSeq annotation was available, the number of autophagy-associated genes found and mammalian order is displayed.

Supplementary Table 10. Autophagy-associated genes tested for selection pressure across eutherian mammals.

Supplementary Table 11. Additional gene data.

Mammalian genome	Number of genes	Order	Reference used
Rhinolophus ferrumequinum	160	Chiroptera	*Rhinolophus sinicus*
Megaderma lyra	100	Chiroptera	*Rhinolophus sinicus*
Eidolon helvum	174	Chiroptera	*Myotis lucifugus*
Pteronotus parnellii	108	Chiroptera	*Myotis lucifugus*
Myotis myotis	254	Chiroptera	*Myotis lucifugus*
Choloepus hoffmanni	168	Xenarthra	*Dasypus novemcinctus*
Procavia capensis	185	Afrotheria	*Loxodonta africana*
Manis pentadactyla	87	Pholidota	*Manis javanica*

A number of additional genomes were mined for autophagy-related genes. These data were included in a separate data set. The reference genome used to annotate each target mammal is displayed.